Journal of Materials Chemistry C

Accepted Manuscript

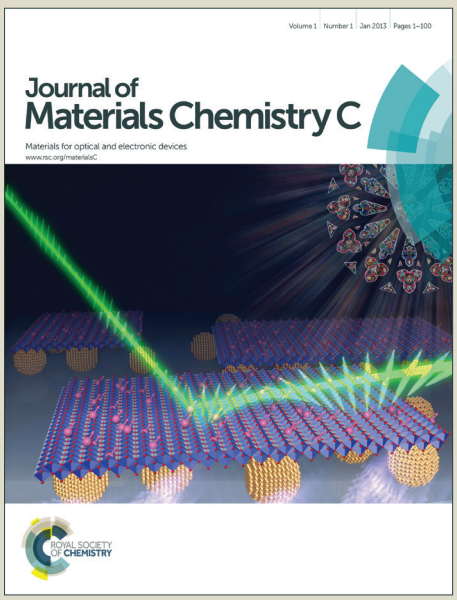

ROYAL SOCIETY OF CHEMISTRY

www.rsc.org/materialsC

Journal of Materials Chemistry C

ARTICLE

Self-powered Flexible Pressure Sensors with Vertically Well-aligned Piezoelectric Nanowire Arrays for Vital Signs Monitoring

Received 00th January 20xx,
Accepted 00th January 20xx

DOI: 10.1039/x0xx00000x

www.rsc.org/

Xiaoliang Chen,[a] Jinyou Shao,*[a] Ningli An,*[b] Xiangming Li,[a] Hongmiao Tian,[a] Chuan Xu[a] and Yucheng Ding[a]

Human vital signs such as the heartbeat and respiration are important physiological parameters for public health care. Precisely monitoring these very minute and complex time-dependent signals in a simple, low-cost way is still a challenge. This study shows a novel fabrication of vertically well-aligned piezoelectric nanowire array with preferential polarization orientation as highly sensitive self-powered sensor for vital signs monitoring. The process realizes *in situ* poling of the P(VDF-TrFE) nanowires within the nanopores of anodized aluminium oxide (AAO) template to yield both preferential alignment of nanowires and the polymer chains required for superior sensitivity using one step. The resulting self-powered flexible sensor shows high sensitivity, good stability and strong power-generating performance. Under bending conditions, the device exhibits the maximum voltage of ~4.8V and current density of ~0.11μA/cm^2. The fabricated self-powered sensor shows a linear relationship of output voltage versus compressive force with a high sensitivity, and the piezoelectric voltage of the P(VDF-TrFE) nanowire array is enhanced to 9 times that from conventional spin-coated bulk film. Furthermore, the highly sensitive vertically well-aligned nanowire array can be applied as a self-powered sensor for detecting some tiny human activities including breath, heartbeat pulse, and finger movements, which may possibly serve for medical diagnostics as sensors, robotics and smart electronic devices.

Introduction

The market of flexible pressure sensors, especially in portable and wearable devices for applications such as artificial skins, health monitors, and biomedical implants are foreseen to skyrocket in the coming year.[1-3] Highly sensitive flexible sensors which can precisely monitor physiological and biomechanical signals of the human body have become a hot research field with the development of medical technology and people's increasing attention to their health.[4-6] Monitoring vital signs, such as the heartbeat and respiration has been considered as an effective approach for physicians to assess the basic functions of human body even at the current age of highly developed medical technology.[7] However, these physiological signals in biological systems are complex time-dependent signals with very minute magnitude and low frequency, which makes them rather difficult to be detected precisely in a simple, low-cost way. The commercial vital sign monitors commonly adopted in the clinical setting can precisely achieve multiple physiological parameters are normally expensive, bulky, and non-portable, and thus, could restrict their application in home healthcare.[8]

In order to facilitate the monitoring of the vital signals, recently, researchers have focused on developing a new technology of utilizing high-sensitive nanostructured materials to directly obtain the subtle signals.[9-13] For example, many wearable pressure sensors based on piezoresistive effect, such as reversible interlocking of nanofibres[10] or graphene woven fabrics[7] as the active layer, have been actively developed and exhibited promising pressure sensing properties. However, bias voltage was inevitable for these sensors during the operation, which would increases the device cost considering external power supply and causes problems such as power consumption and structural complexity.[14] Alternatively, the pressure sensors based on piezoelectric effect can simplify the device unitizing their unique self-powered characterization which makes electronic device packages possible forgoing the inclusion of bulky battery components.[15-19] Since the first piezoelectric ZnO nanogenerator was proposed in 2006,[20] piezoelectric nanowires are particularly attractive for self-powered sensing devices due to their robust mechanical properties and high sensitivity to small forces.[21] Compared to the conventional bulk-film structure, the one dimensional nanowires enable much larger critical strain, higher flexibility, and longer operational lifetime. In this framework,

[a] *State Key Laboratory for Manufacturing Systems Engineering, Xi'an Jiaotong University, Xi'an, Shaanxi 710049, China.*
E-mail: jyshao@mail.xjtu.edu.cn (Jinyou Shao).
[b] *College of Printing and Packaging Engineering, Xi'an University of Technology, Xi'an, Shaanxi 710048, China.*
E-mail: annl@xaut.edu.cn (Ningli An)
Electronic Supplementary Information (ESI) available: See
DOI: 10.1039/x0xx00000x

polymer based piezoelectric nanomaterials, such as the PVDF or its copolymer P(VDF-TrFE) combine structural flexibility, processing simplicity with excellent chemical stability, and good biocompatibility, making them competitive for high-sensitive sensors for vital signs monitoring.[22-25] For achieving good output performance, these piezoelectric polymers require electrical poling to create maximum polarization in the direction orthogonal to the film plane,[26] which requires multiple steps and constrains engineering design options.[27] Most recently, electrospinning methods based on electrohydrodynamic deformation (EHD) have been exclusively presented to produce piezoelectric nanofibers of PVDF and its copolymers, in which the drawing force and electric field naturally cause local poling during nanofabrication.[28-33] The fabricated nanofibers of PVDF by this way are most either in the form of non-woven mats with modest degrees of alignment[32, 33] or single electrospun PVDF nanofiber.[30, 34] These fibers often require high-electric fields for poling, provided by either post-poling [31] or near field electrospinning which requires sophisticated equipment.[30] Furthermore, these horizontal aligned PVDF fibers were most laterally deposited on a flexible substrate, which would require a large bending of the substrate to produce an adequate stretching of the fibers and largely damp the magnitude of the mechanical triggering, and thus, limit their performance as high-sensitive pressure sensor. In reality, high sensitive sensing device functionality under low magnitude pressure situation can be best achieved with high volumetric densities of vertically aligned arrays of flexible nanowires, because the low magnitude pressure acted directly onto the sensing nanowires structure without being damped by the packaging material or substrate. However, the previous fabrication process often suffers from poor control over large area piezoelectric polymer nanowires with large aspect ratio, high degrees of alignment in the vertical direction and uniformity in coverage.[35-39]

In this paper, a new nanotemplate-based electricity-grown method was proposed to fabricate the vertically well-aligned P(VDF-TrFE) nanowire array with the desired crystal and preferential polarization orientation, which show an excellent performance on sensing application for vital signs monitoring. In our strategy, an electrical voltage is applied to an electrode pair composed of a conductive nanoporous anodized aluminium oxide (AAO) template and a P(VDF-TrFE) film coated-conductive substrate, generating an electrodynamic force to grow and *in situ* pole the P(VDF-TrFE) nanowires within the nanopores. The nanotemplate-induced space confinement promotes preferential alignment of the polymer dipoles and the nanowires along the vertical direction. Under bending conditions, the device exhibits the maximum voltage of ~4.8V and current density of ~0.11μA/cm^2. The piezoelectric voltage of the P(VDF-TrFE) nanowire array was enhanced to 9 times that from conventional spin-coated bulk film under the same compressive force. The fabricated device also showed a linear relationship of output voltage versus compressive force with a high sensitivity. Furthermore, we show that the highly sensitive self-powered sensor can be used to detect some tiny human activities including breath, heartbeat pulse, and finger movements, which shows its potential application in personal health monitor.

Results and Discussion

Fabrication of the vertically well-aligned P(VDF-TrFE) nanowire array as self-powered pressure sensor.

Fig. 1a illustrates the processes for fabricating a self-powered flexible pressure sensor (SFPS) by electrohydrodynamic deformation (EHD) of the P(VDF-TrFE) polymer within the nanopores of AAO template. Generation of the free standing P(VDF-TrFE) nanowire array starts with pressing AAO nanoporous templates (the conductive Al backup as upper electrode) against P(VDF-TrFE) film-coated flexible conductive substrate (Au-coated Kapton thin film in our experiment, as the lower electrode), as shown in Fig. 1a-i. The assembly is then thermally maintained at a temperature of 160°C, which is higher than the melting temperature of P(VDF-TrFE) (T_m=150°C), while a DC voltage of 500V is applied between the template and substrate (Fig. 1a-ii). The electrical voltage applied across the electrode pair, generating an electrodynamic force acting on the polymer surface, driving the polymeric liquid flow upward along the solid wall of template. While the polymeric liquid undergoes an axial extension during the deformation, the molecular dipoles inside the polymer can be expected to be aligned vertically due to the combined thermoplastic and EHD effect, as the yellow arrows shown in Fig. 1a-ii. After an annealing time for the polymer fully filling within the nanopores, a slow cooling of the sample to room temperature cures the nanostructures, inducing a re-crystallization of the P(VDF-TrFE) nanowire array at the same time. The vertically well-aligned free-standing P(VDF-TrFE) nanowire array is obtained after dissolving the AAO template, as shown in Fig. 1a-iii. In our experiment, the Al layer is first removed by immersing the sample in a mixture of 2mol/L $CuCl_2$ solution in water and 36wt.% HCl solution in water) ($CuCl_2$ solution: HCl solution 2:1 in volume). The Al layer has a thickness of ~200μm (as shown in the Supplementary Information, Fig. S1) and can be completely removed after 5-6min. After that, by dissolving the sample in 4 mol/L NaOH solution in water for 30-40min, the aluminium oxide layer can be dissolved. To fabricate the SFPS, a thin layer of PMMA is spin-coated onto top of the nanowires to avoid the short circuit of the device and followed by spinning a conducting polymer poly(3,4-ethylenedioxythiophene):poly(styrenesulfonate) (PEDOT:PSS) as the top flexible electrode. The entire flexible device is made of vertically well-aligned piezoelectric P(VDF-TrFE) nanowire array sandwiched between two flexible electrodes, as shown in Fig. 1b. Fig. 1c shows an optical image of a bent SFPS device which has an effective area of 10mm×10mm, indicating a large flexibility of the device. Fig. 1d provides a SEM image at a cross section of the SFPS device. These sandwiched nanowires are high degrees of alignment in the vertically direction, showing a final diameter of about 400nm and 10μm in length, reflecting the template matrix features. The initial thickness of the spin-coated P(VDF-TrFE) layer was about 8-9μm. After the fabrication of nanowire array, a thin layer of polymer

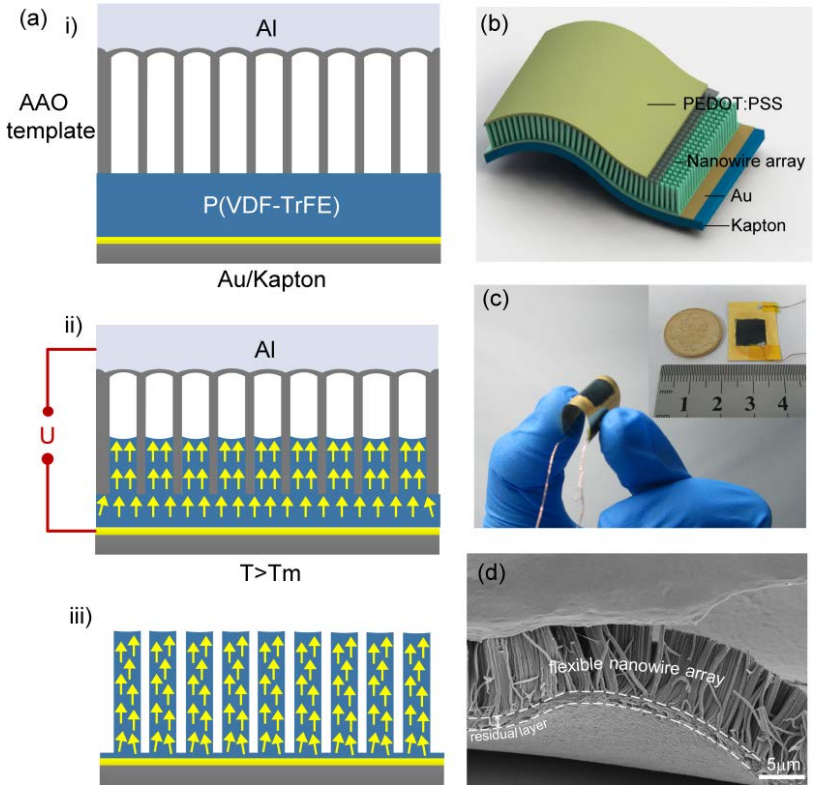

Fig. 1 (a) Experimental steps for building SFPS. (b) Scheme of the flexible piezoelectric device. (c) The Optical image of a bent SFPS sample. (d) SEM images of cross section of the SFPS device. A thin layer of polymer remains as a film underneath the nanowire array, as denoted by the white dotted line. Scale bars: 5μm.

which has a thickness of about 2 μm remains as a film underneath the nanowire array, as denoted by the white dotted line in Fig 1d. For the remaining thin film, the degree of the dipole orientation inside the material depends on the thickness and processing temperature, etc.[40] Therefore, the thin remaining film is functioned as the flexible supporting layer and the outputs of the device are mainly from the piezoelectric nanowire array.

The proposed template-based electricity-grown method here is an *in situ* poling fabrication progress which the nanostructure fabrication and electrical poling are synchronously accomplished in a single-step procedure. Fig. 2a presents an intermediate snapshot for the dynamic deformation of the liquefied polymer flow upward along the solid wall of nanotemplate, which is obtained by a numerical simulation based on an electrohydrodynamic formulation of the liquid-air phase-field problem in our previous publication.[41] The detailed simulation progress can be seen in Fig. S2. It is important to note that the directions of the electric field inside the nanowire are always dominantly along the axis of the nanowire throughout the nanowire flowing within the nanopore (as the yellow arrows shown in Fig. 2a), which is benefit to align the electric dipoles in the vertical direction for achieving the super piezoelectric performance. The average electric intensity inside the nanowire increased during the flowing process until the nanowire fully filling within the nanopore, then it keep on a maximum value, as shown the red dotted line in Fig. 1e. Therefore, to better align dipoles in the P(VDF-TrFE) nanowire array, it is necessary to maintain the temperature and voltage for a period time (about 1 hour in our experiment), and then slowly cooling the material, while still in the electricity field, for "freezing" the dipoles in place. So in our proposed method, the electricity-grown of P(VDF-TrFE) nanowires and *in situ* poling of the vertically aligned nanowires accomplished in one step. Fig. 2b shows the fabricated free-standing P(VDF-TrFE) nanowire array after releasing from the nanoporous template. The vertical alignment of the P(VDF-TrFE) nanowires was enforced by the nanopores of the AAO template, resulting in a high degrees of vertically alignment and better uniformity in coverage than nanofibers fabricated by electrospinning.

Interestingly, we find that the P(VDF-TrFE) nanowires fully crystallize into the β-phase in the nanoporous matrix, whereas the reference bulk film of P(VDF-TrFE) partially crystallizes in the α nonpolar phase. The preferential crystal structure of the nanowire array was demonstrated by X-ray diffraction (XRD) measurements which carried out at 2θ angles from 10°to 50°. Fig. 2c shows the XRD pattern recorded on nanowire array (bottom red line) resulted from the AAO nanoporous template and that of P(VDF-TrFE) bulk film (top blue line). The prominent peak at 19.9°corresponds to overlapping of (110) and (200) Bragg reflections of ferroelectric β phase of P(VDF-TrFE) which exist on both nanowires and film

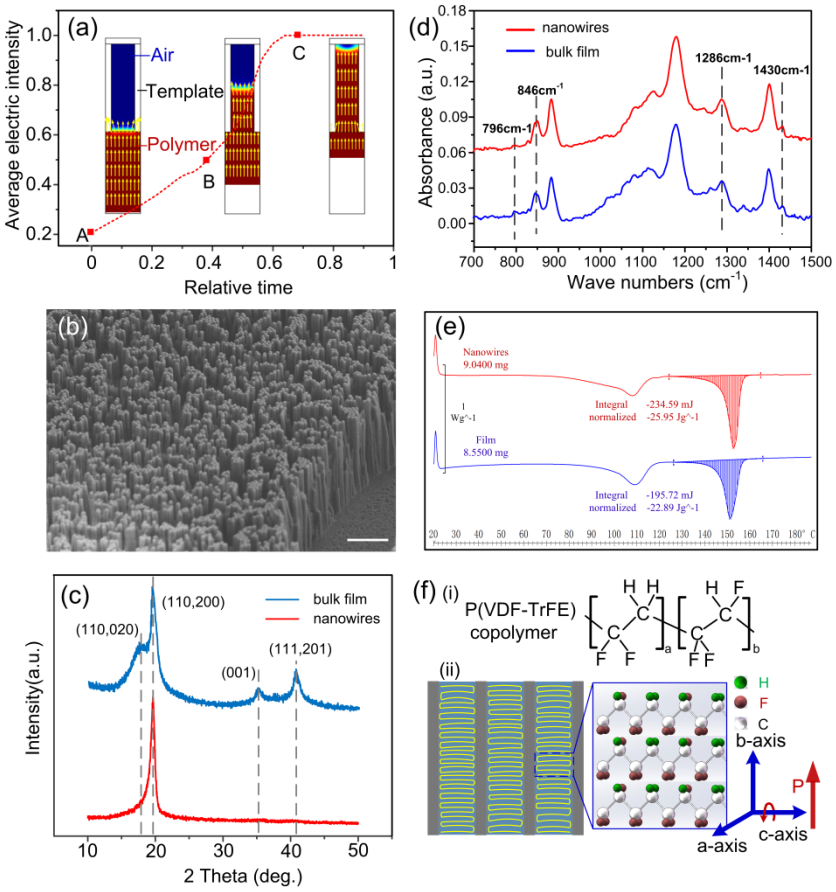

Fig.2 (a) The vectored electric field (denoted by the yellow arrows) and the average electric intensity (denoted by the red curve) inside a P(VDF-TrFE) nanowire during its deformation within the nanopores of AAO template. (b) The SEM of freestanding P(VDF-TrFE) nanowire array fabricated by the template-based electricity-grown method after releasing from the nanoporous template. (c) XRD patterns from a bulk P(VDF-TrFE) film (top blue line) and vertically aligned P(VDF-TrFE) nanowire array (bottom red line).The polar β-phase is dominant in the nanowire XRD spectrum. The bulk film shows a mixture of α and β phases in comparison.(d) ATR-FTIR spectrograms of P(VDF-TrFE) nanowires and bulk film. The red curve was moved upwards 0.06 units. (e) DSC scans results of P(VDF-TrFE) nanowires and bulk film. (f) (i) The chemical formula of P(VDF-TrFE) copolymer; (ii) schematic representation of the polymer chain molecular orientation in the AAO membrane, red: F, green: H, white: C. Inside the porous alumina the b-axis of the crystal unit cell is aligned parallel to the long axis of the nanowires with the a- and c-axes lying on the cross section of the nanowires, perpendicular to its long axis. Scale bars: 5μm.

samples. The bulk film reference sample shows several diffraction peaks belonging to the α nonpolar phase at 18.4 and 40.7°, respectively corresponding to the (110), (020) reflections and to overlapping of (111) and (201) reflections,[42] whereas the nanowires sample did not show any clear peak. The polymeric crystallinity of the P(VDF-TrFE) nanowires was further examined by Fourier transformed infrared spectroscopy (FTIR) spectra in ATR mode over a range of 700-1500 cm^{-1} with a resolution of 2 cm^{-1}. As shown in Fig. 2d, the polar β-phase bands appear distinctly at 846, 1286 and 1430 cm^{-1}. Meanwhile, the very low absorbance bands at 796 cm^{-1} correspond to the low content of α-phase.[43] In order to determine the β-phase content present in each sample, infrared absorption bands at 796 and 1286 cm^{-1}, characteristics of the α- and β-phases, respectively.[44] Assuming that the FTIR absorption follows the Lambert-Beer law, the fraction of β-phase F(β) in the material can be calculated using[45]:

$$F(\beta)=\frac{X_\beta}{X_\alpha+X_\beta}=\frac{A_\beta}{1.26A_\alpha+A_\beta}$$

where A is the absorbance of the α and β phases with absorbance peaks at 796 cm^{-1}, 1286 cm^{-1}, respectively. By analysis the FTIR results, the P(VDF-TrFE) nanowires showed high contents of β-phase about 83.5%, compared with a β-phase fraction of 75.2% for bulk film. This result indicates that crystallization of the nanowires into the β-phase was enhanced, which confirms the XRD results. This is consistent with recent studies which show that a higher proportion of the β crystalline phase in template-grown P(VDF-TrFE) nanowires and preferential orientation of the crystal lamellae occur solely due to the confinement effect of the nanoporous template.[37, 46] For characterizing the crystallinity of P(VDF-TrFE) polymer,

sections of the P(VDF-TrFE) nanowire array and bulk film for differential scanning calorimetry (DSC) characterization were subjected to thermal analysis under a flowing nitrogen atmosphere between 20 and 200 °C and at a heating rate of 10 °C min^{-1} using a METTLER instrument. The Fig. 2e shows the DSC scans results. Two peaks are identified where the first peak corresponds to the ferroelectic-to-paraelectric transition, identified by T_{fp}, and the second peak represents the melting transition, T_m. The degree of crystallinity (ΔX_c) of the samples was calculated from the DSC scans using:

$$\Delta X_c = \frac{\Delta H_m}{\Delta H_0}$$

where ΔH_m is the melting enthalpy of the sample and ΔH_0 is the melting enthalpy for a 100% crystalline sample. The 100% crystallinity values of P(VDF-TrFE) used to calculate the crystallinity is 45 J g^{-1}.[47, 48]

Table 1. DSC parameters of P(VDF-TrFE) nanowires and bulk film

P(VDF-TrFE)	T_{fp}(℃)	T_m(℃)	ΔH_m (J/g)	ΔH_c (%)
Nanowires	108.2	152.9	25.95	57.7
Bulk film	109.3	151.3	22.89	50.8

As shown in the Table 1, the calculated results indicate that the crystallinity of the material in the nanowire array is ~57.7%, while that for the bulk film is 50.8%. Therefore, taking advantage of the confinement of the porous alumina channels, the P(VDF-TrFE) nanowires obtained a high degree of crystallinity.[49]

The amplified SEM images of the nanowires of P(VDF-TrFE) are shown in the Fig. S3. The needle-like grains were observed in the interior of nanowires, as denoted by the dotted line circles. This long narrow shape of needle-like grains has also been observed in Guo *et al.*'s studies.[50, 51] According to their research, the ultrathin P(VDF-TrFE) films showed a distinct granule toward layered needle-like network (LNN) morphology transition with increasing annealing temperature.[51] So the needle-like grains observed in our samples may result from the greatly enhanced mobility of the macromolecule segments in the molten state. It seems that these needle-like crystals were not randomly oriented but stacked along the polymeric nanowires and set perpendicularly to longitudinal axis of the nanowires. Because the a-and c-axes are in plane with the crystalline lamellae and the b-axis is perpendicular to them, so this arrangement of needle-like crystals can also confirm the polymer chain molecular orientation within the nanowire structure.[37] By now, various authors have reported the effect of nanoconfinement on PVDF crystallization, which leads to preferential orientation of the crystal lamellae.[35] When PVDF, or its copolymer P(VDF-TrFE) were templated into anodic porous alumina, the nanoconfinement effect of the alumina nanopore will induce the lamellar crystals grow preferentially flat on the templating surface channel to accommodate the confined environment of the nanotemplate, resulting in a preferential crystal orientation that the polarization b-axis of the polymer parallel to the long axis of the template. This mechanism has been confirmed by the molecular simulations[52, 53]and many experimental studies in previously reported literatures.[37, 54, 55] Therefore, combine with the experiment results and the literature reports[35, 37, 39, 54, 55], a schematic illustration of the most possible speculation about the polymer chain molecular orientation is presented in the Fig. 2f. Inside the porous alumina, the b-axis of the crystal unit cell is aligned parallel to the long axis of the alumina channel with the a- and c-axes lying on the cross section of the template, perpendicular to its long axis. So upon the application of a vertical electric field coaxial to the alumina channels during the fabrication of nanowires as shown in Fig 1a-ii, the dipole moment of polymer can easily rotate around about the horizontal chain c-axis, as denoted by the red arrow. Therefore, the polarization P will be maximized along the long axis of the nanowires owing to the vertical orientation of the polar b-axis.[56] In a recently excellent review[57] about the fabrication and performance of ferroelectric polymer nanostructures, Guo *et al.* point out that nanoconfinement usually leads to preferential orientation of the polymer chains, which in turn may give rise to improve the ferroelectricity and piezoelectric response along the molecular dipole alignment direction. So further studies will be carried out to confirm the definite information of dipole orientation in the nanowires by in-plane XRD or in-plane IR characterization techniques,[58, 59] which may be help us to better understand the enhanced sensitivity of the nanowires based-devices.

Sensing performance of the SFPS devices response to bending and compressive forces.

To study the output performance of the SFPS under bending deformation, the device is periodically deformed by a linear motor with a maximum horizontal displacement of 10mm at an average deformation rate of 10mm/s (Fig. 3a), and the generated electrical piezoelectric voltage and current signals are shown in Fig. 3a,b. Under the continual bending and releasing cycles, the SFPS device with an effective area of 10mm×10mm repeatedly generates the maximum voltage of ~4.8 V and an average current density of ~0.11μA/cm^2, which are higher than the output of previously reported nanowires-based P(VDF-TrFE) nanogenerators.[32, 43, 60] To verify that the measured signals were indeed generated by the SFPS sample as a whole, a widely accepted switching-polarity test was conducted. In the forward connection, the device generates a negative voltage and current upon the bending states (Fig. 3a,b). On the contrary, in the case of the reverse connection, the positive output pulses are measured, as shown in Fig. S4. The results indicated that the measured outputs were the true signals coming from piezoelectric responses instead of artificial effects. The sensing mechanism of vertically aligned P(VDF-TrFE) nanowire array can be understood in terms of piezoelectric polarization under mechanical deformation. During the bending action, the nanowires layer is compressively strained and a positive piezoelectric potential is developed at the top side of the nanowires, as shown in Fig. 3c-i. The piezopotential difference induces free electrons started to flow from the bottom electrode to the top electrode through an external circuit, giving a negative electric output. Since the piezoelectric potential is balanced by the free electrons from external circuitry at a constant strain, no visible voltage signal appears during holding.

Subsequently, when the strain is released, the positive voltage was observed due to the piezoelectric potential fade away and the electrons accumulated near the top electrode tend to move back to their original positions, as shown in Fig. 3c-ii. Being different from the reported triboelectic nanogenerators[61, 62] which employed a typical structure consisting of a pair of friction surfaces to produce triboelectic charges and an air gap to change the distance between the friction surfaces to produce electricity, our piezoelectric device was an entire whole structure which is made of vertically aligned piezoelectric P(VDF-TrFE) nanowire array sandwiched between two flexible electrodes. The whole structure was flexible and didn't separate during the deformation. Therefore, there is no air gap between the electrodes and nanostructures to induced apparent triboelectic charge. So the voltages generated by our samples are truly due to the piezoelectric contribution, but not from a triboelectric contribution. The strain-dependent property of a device was evaluated by deforming the sensor under different horizontal displacement from 2mm to 10mm. As shown in Fig. 3d, the amplitude of the output voltage increases from 1.2 V to 4.8V with the bending curvature because the internal piezoelectric potential can be enhanced by the introduced strain. The stability of the sensor was examined by continually bending and releasing motions with a maximum horizontal displacement of 10mm at an average deformation rate of 10mm/s. The sensor device shows good mechanical robustness and stability, and the voltage amplitudes shows only a slight fluctuation after 8000s, as shown in the Fig. 3e. The inset figures show the magnified outputs at the beginning and the end of the test. This stable output performance can be attributed to the robust mechanical property of the nanowires structures under significant deformation and the entire flexibility structure design.

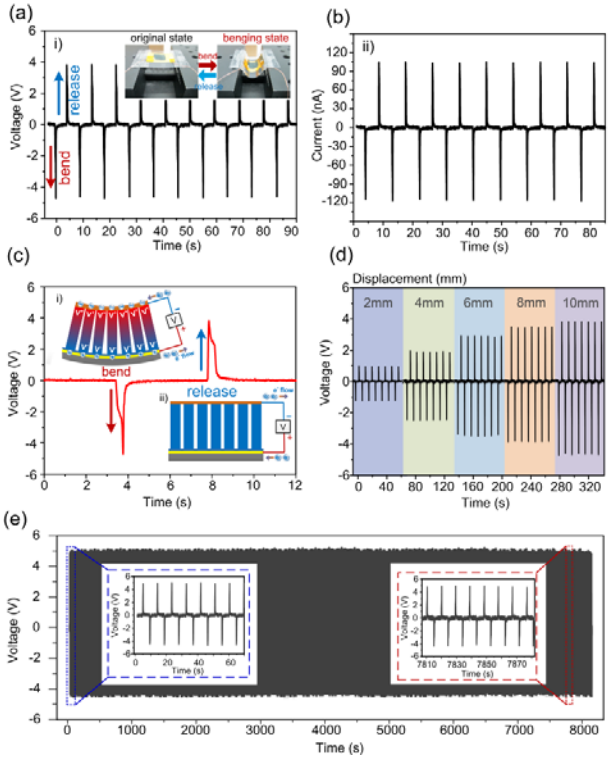

Fig. 3 Output responses as flexural sensor. (a,b) Upon the repeatedly bending/release motions, the corresponding output voltage/current time curves, the inset of (a) shows the captured images of an device at original and bending states. (c) The sensing mechanism of vertically aligned P(VDF-TrFE) nanowire array under mechanical bending deformation. (d) The piezoelectric output of the device under different horizontal displacement from 2mm to 10mm.(e) The output stability of the sensor was examined by continually bending and releasing motions.

In order to characterize the sensing performance of the device under vertically applied compressive force, an experimental set-up was designed. Fig. 4a represents a block diagram of the set-up, and Fig. 4b shows a photograph of the experimental setup. The SFPS was positioned under a cylindrical probe, which was driven by an electromechanical vibrator, with some detailed information included in the Fig. S5. Fig. 4c-i shows typical output voltage of the device when impacted with vibrations of a peak force of 2.5N at frequency of 2 Hz. The output voltage has the same frequency as that of the applied force and the maximum output voltage reaches 1.1V. Importantly, the voltage amplitudes revealed no significant declining over continuous impacting nearly 5h (≈36000 cycles) (Fig. 4c-ii), indicating that the SFPS device have an excellent mechanical robustness and stability. The sensing performance of the SFPS device was demonstrated by applying periodic vertical force range from 0.1N to 4N to the top of the device in the vertical direction. The relationship between output voltage and applied force is shown in Fig. 4d, showing that the output voltage increases linearly with force. The achieved slopes of the sensor are 458.2mV/N, which has been largely improved than our previous publication.[63] We also compared the sensing performance under different electrical poling process with external voltage from 100 to 500V, as shown in the section of Fig. 4d. The generated voltages of device increase with external pulling voltage. This output behaviour is the typical piezoelectric effect, which also confirms that the measured outputs were the true signals coming from piezoelectric responses instead of artificial effects or triboelectric effect.

In order to demonstrate a higher sensitivity improved by the vertically well-aligned nanowire array, we compared the output voltages from two nanowire based devices with that from a bulk film-based device generated using the same poling nominal electric field intensity (i.e. some voltage per unit gap of the electrode pair, 50V/μm in our experiment). The device with the nanowire array of a low aspect ratio has a diameter of ~400nm and a height of ~5μm for the nanowires (Fig. 4e-I), and the one of a high aspect ratio has a diameter of ~400nm and a height of ~10μm (or Fig. 4e-II). The bulk film has a thickness of 10μm and an area of 10 mm×10mm for an objective comparison. Piezoelectric output voltage with a maximum value of 0.2, 0.9, and 1.8V from the bulk film, nanowires (I), and nanowires (II) were obtained under the same vertical compressive force of 4N, as shown in Fig. 4e. The output voltage of nanowire-based device showed high value nearly nine times of enhancement compared to the bulk film-based device. The superior

performance can be attributed to the geometrical strain confinement of the nanowire structure, enhanced ferroelectric phase formation and preferential oriented crystallization formed from nanoconfinement in template nanopores.[46, 64, 65] Using such a high sensitive nanowire array, we further show its strong power generating ability of converting no-contact air flow into electricity, which can be used to drive commercial light emitting device (LED), and liquid crystal display (LCD), as shown in Fig. S6 and Supplementary Video1.

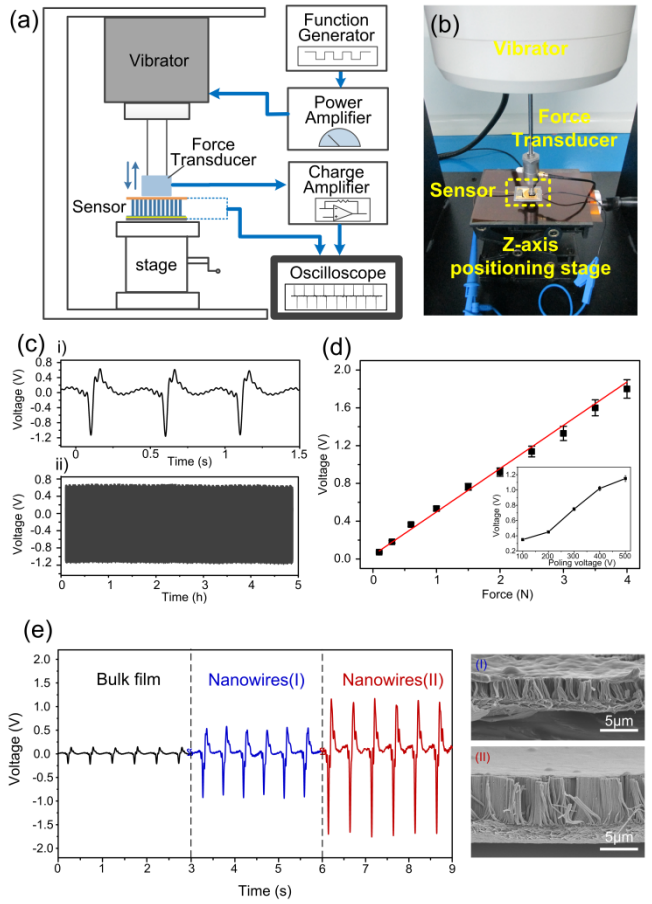

Fig. 4 (a) Schematic diagram of the experimental setup used in the piezoelectric sensing measurements. (b) Photograph of the experimental setup. (c) Typical output voltage characteristics of the SFPS (i) and five hours (~36000 cycles) continuous power generation of the device (ii). (d) The relationship between output voltage and applied force from 0.1N to 4N. The inset shows the output performance under different electrical poling process with external voltage from 100 to 500V. (e) A comparison of output voltages for SFPS based on nanowires with two aspect ratios and for a bulk P(VDF-TrFE) film; the right inset shows SEM images for the nanowires with two aspect ratios. Scale bars: 5 μm.

SFPS device used for human activity monitoring

To demonstrate the application of the device as human activity monitoring sensor, the SFPS device was first fixed on a finger to detect the finger motion states. At the beginning, the finger remains still, no response was detected, as shown in Fig. 5a-I. When the finger moved with a little amplitude, the deformation sensor would response, as shown in Fig. 5a-II. Once the moving amplitude was larger, a higher output voltage was observed, like the output peak of Fig. 5a II-Vi. This is because the larger the bending amplitude, the larger the applied bending strain is on the nanowires, therefore generating more output voltage. This study indicated that the SFPS device can be used as a strain sensor for detecting muscle motion and has potential application in patients' rehabilitation training. Because the vertically well-aligned P(VDF-TrFE) nanowire array exhibits high sensitivity in response of small force, the SFPS device even could be used for detecting the breathing of human. All the applications of health monitoring were carried out with the nanowire-based sensor of 10μm in thickness. In order to avoid interference caused by other stimulation, the sensor was fixed on a glass substrate and put under the nose. When blowing onto the sensor by a gentle breathing, an average output voltage of 0.2V was observed. The output curve under several breathing cycles is shown in Fig. 5b. The real-time output of the sensor was recorded in response to the breathing behavior (Supplementary Video2). This study indicated that the SFPS device can be used as a breathing sensor in biomedical and health-care applications. Another practical application is a heartbeat-pulse sensor. The pulse is one of the output signals of a human heart system, which is a complex time-dependent signal reflecting the fluctuation of one's motion and health situation.[11] Our vertically aligned nanowire based sensor can be used to take those vital signs. As shown in the section of Fig. 5c, the SFPS was attached to the wrist by finger to get the *in-situ* original blood pressure signal. The output of the sensor was recorded in response to the heart-beating behavior (Supplementary Video3). The output results completely complied with the realistic physiological behaviors. As shown in Fig. 5c, the pulse numbers are average 78-80 in 60s, which is within the normal range of a healthy adult. Last, in order to demonstrate the high sensitivity of the SFPS in a low magnitude situation, we measured the output of this sensor upon they are exposed to sound waves, as shown in the section of Fig. 5d. Compared to the pressure on the contact-mode, the sound pressure applied on the surface of device is extremely small. Pressure of the sound at 100 dB is only 2 Pa.[66] We clearly observed a voltage output even upon the exposure of the device to sound waves with a low input power of 85dB, clearly tells us that nanowire based device is prominently suitable for detecting minuscule stress.

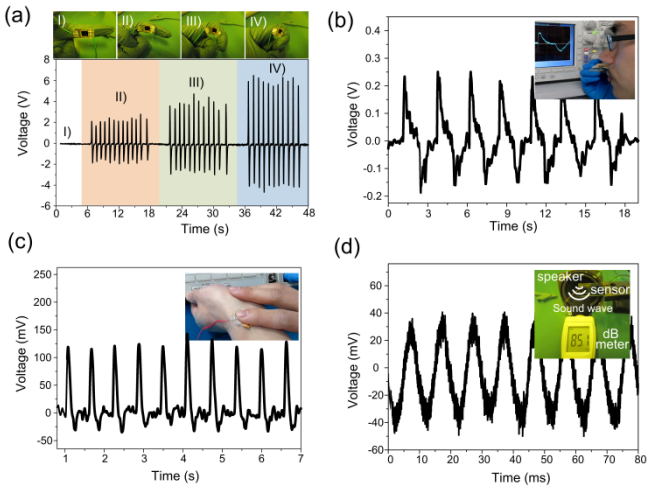

Fig. 5 The SFPS device used for detecting finger motion states (a), breathing (b), heartbeat(c) and low magnitude sound waves (d).

Conclusion

In summary, we have proposed and successfully demonstrated a novel template-based electricity-grown method for fabricating vertically aligned P(VDF-TrFE) nanowire array, which has been demonstrated as a self-powered high-sensitive pressure sensor for monitoring vital signs. The fabrication process realizes *in situ* poling of the P(VDF-TrFE) nanowire within the nanopores of AAO template to obtain the preferential oriented β crystalline phase, thereby enabling high sensitivity piezoelectric output without further electrical poling. Under the continual bending and releasing cycles, the SFPS device with an effective area of 10mm×10mm repeatedly generates the maximum voltage of ~4.8V and current density of ~0.11μA/cm^2, showing its strong power-generating performance. In addition, the performance of the piezoelectric nanowire array as a self-powered pressure sensor was demonstrated under vertical compressive force test. The *in situ* poled nanowire-based sensor reveals nearly 9 times larger voltage output compared to a bulk film-based sensor. The SFPS device also showed a linear relationship of output voltage versus compressive force with a high sensitivity. Alongside high sensitivity, the cycling stability of the present sensor has been demonstrated to output repeatable and reproducible signal over 36000 cycle tests. Finally, the highly sensitive nanowire arrays demonstrated the potential to work as a self-powered pressure sensor to detect the subtle pressure and some weak human activities including breath, heartbeat pulse, finger movement and low magnitude sound wave. Because of the distinctive features of high sensitivity, good stability and strong power-generating performance, the SFPS device described here will have a wide potential application in fields of the robotics, body monitoring, in vitro diagnostics, and smart electronic devices.

Experimental Section

The detailed fabrication progress of the SFPS. P(VDF-TrFE) solution was prepared by dissolving P(VDF-TrFE) powder with a molar ratio of 70/30 (purchased from Kunshan Hisense Electronics Co.,Ltd) in N,N-dimethylformamide (DMF) with stirring for 1 h in heated water bath at a temperature of 60°. Films of P(VDF-TrFE) were made by spin-coating on flexible Au-coated Kapton substrate, followed by annealing at 125°C for 2 h to remove the DMF solvent. The nanowire arrays with two different aspect ratio were prepared by electricity-grown P(VDF-TrFE) film with commercially available anodic aluminum oxide (AAO) nanoporous templates (Shanghai Shangmu Technology Co. Ltd) with 400 nm pore diameter and 5μm,10μm pore length, respectively. The free standing P(VDF-TrFE) nanowire array was obtained after dissolving the AAO template in 4 M NaOH solution in water. The conducting polymer poly(3,4-ethylenedioxythiophene):poly(styrenesulfonate) (PEDOT:PSS) 1.0 wt. % in H_2O was purchased from Sigma–Aldrich.

Measurement and Characterization. The electrical output signals from the SFPS devices were recorded by the Tektronix DPO3034 oscilloscope. The output voltage was measured with a 100MΩ probe and the output current was measured using low-noise current preamplifier (Model No. SR570, Stanford Research Systems, Inc.) The sound wave was generated by a speaker using a function generator (Agilent 33220A). The magnitude of the generated sound wave was measured by digital sound level meter AS804.The DC voltage used in the thermopoling and EHD process was applied by an amplifier/controller (TREK 610E H.V.). All the SEM images were captured using a HITACHI SU8010 SEM instrument. Wide-angle X ray diffraction patterns were collected on a SmartLab X-ray diffraction system with Cu-Kα radiation at λ = 1.5418 A. The experiment setup was in θ–2θ mode, having the scattering vector perpendicular to the sample surface. The scanning 2θ range was 10°to 50°, with a scanning speed of 5°/min. The sampling pitch was 0.02° and the present time 0.24s. The X-ray generator was operated at 40kV and 40mA. The phase of the P(VDF-TrFE) nanowires was examined by Fourier transformed infrared spectroscopy (FTIR) spectra using a Bruker VERTEX 70 in ATR mode over a range of 700-1500 cm^{-1} with a resolution of 2 cm^{-1}, 128 scans were performed to each sample.

Acknowledgements

This work is financed by the NSFC Major Research Plan on Nanomanufacturing (grant no. 91323303), and NSFC Funds (grant no. 51275401 and 51305347) and Program for New Century Excellent Talents in University of Ministry of Education of China (NCET-13-0454).

Notes and references:

1 J. Zhong, Q. Zhong, Q. Hu, N. Wu, W. Li, B. Wang, B. Hu and J. Zhou, *Adv. Funct. Mater.*, 2015, **25**, 1798-1803.

2 B. Meng, X. Cheng, X. Zhang, M. Han, W. Liu and H. Zhang, *Appl. Phys. Lett.*, 2014, **104**, 103904.

3 M. Han, B. Yu, G. Qiu, H. Chen, Z. Su, M. Shi, B. Meng, X. Cheng and H. Zhang, *J. Mater. Chem. A*, 2015, **3**, 7382-7388.

4 Y. Jiang, H. Hamada, S. Shiono, K. Kanda, T. Fujita, K. Higuchi and K. Maenaka, *Procedia Eng.*, 2010, **5**, 1466-1469.

5 C.-S. Hu, Y.-F. Chung, C.-C. Yeh and C.-H. Luo, *J. Evidence-Based Complementary Altern. Med.*, 2011, **2012**.

6 T. Gao, J. Liao, J. Wang, Y. Qiu, Q. Yang, M. Zhang, Y. Zhao, L. Qin, H. Xue and Z. Xiong, *J. Mater. Chem. A*, 2015, **3**, 9965-9971.

7 Y. Wang, L. Wang, T. Yang, X. Li, X. Zang, M. Zhu, K. Wang, D. Wu and H. Zhu, *Adv. Funct. Mater.*, 2014, **24**, 4666-4670.

8 Y.-Y. Chiu, W.-Y. Lin, H.-Y. Wang, S.-B. Huang and M.-H. Wu, 2013.

9 G. Schwartz, B. C.-K. Tee, J. Mei, A. L. Appleton, D. H. Kim, H. Wang and Z. Bao, *Nat. Commun.*, 2013, **4**, 1859.

10 C. Pang, G.-Y. Lee, T.-i. Kim, S. M. Kim, H. N. Kim, S.-H. Ahn and K.-Y. Suh, *Nat. Mater.*, 2012, **11**, 795-801.

11 Z. Li and Z. L. Wang, *Adv. Mate.r*, 2011, **23**, 84-89.

12 H. B. Yao, J. Ge, C. F. Wang, X. Wang, W. Hu, Z. J. Zheng, Y. Ni and S. H. Yu, *Adv. Mater.*, 2013, **25**, 6692-6698.

13 R. Li, B. Nie, P. Digiglio and T. Pan, *Adv. Funct. Mater.*, 2014, **24**, 6195-6203.

14 G. Zhu, W. Q. Yang, T. Zhang, Q. Jing, J. Chen, Y. S. Zhou, P. Bai and Z. L. Wang, *Nano lett.*, 2014, **14**, 3208-3213.

15 G. T. Hwang, H. Park, J. H. Lee, S. Oh, K. I. Park, M. Byun, G. Ahn, C. K. Jeong, K. No, H. Kwon, S. G. Lee, B. Joung and K. J. Lee, *Adv. Mater.*, 2014, **26**, 4880-4887.

16 Z. L. Wang, *Adv. Funct. Mater.*, 2008, **18**, 3553-3567.

17 C. K. Jeong, K.-I. Park, J. H. Son, G.-T. Hwang, S. H. Lee, D. Y. Park, H. E. Lee, H. K. Lee, M. Byun and K. J. Lee, *Energy Environ. Sci.*, 2014.

18 M. Lee, J. Bae, J. Lee, C.-S. Lee, S. Hong and Z. L. Wang, *Energy Environ. Sci.*, 2011, **4**, 3359.

19 S. Xu, Y. Qin, C. Xu, Y. Wei, R. Yang and Z. L. Wang, *Nat. Nanotechnol.*, 2010, **5**, 366-373.

20 Z. L. Wang and J. Song, *Science*, 2006, **312**, 242-246.

21 X. Wang, *Nano Energy*, 2012, **1**, 13-24.

22 S. Choi and Z. Jiang, *Sens. Actuators, A*, 2006, **128**, 317-326.

23 S. Kärki and J. Lekkala, 2008.

24 Y. Xin, X. Qi, C. Qian, H. Tian, Z. Ling and Z. Jiang, *Integr. Ferroelectr.*, 2014, **158**, 43-51.

25 M. Han, X.-S. Zhang, B. Meng, W. Liu, W. Tang, X. Sun, W. Wang and H. Zhang, *ACS nano*, 2013, **7**, 8554-8560.

26 A. Shirinov and W. Schomburg, *Sens. Actuators, A*, 2008, **142**, 48-55.

27 P. Martins, A. C. Lopes and S. Lanceros-Mendez, *Prog. Polym. Sci.*, 2014, **39**, 683-706.

28 Y. Ding, Y. Duan and Y. Huang, *Energy Technology*, 2015.

29 Y. Huang, Y. Duan, Y. Ding, N. Bu, Y. Pan, N. Lu and Z. Yin, *Sci. Rep.*, 2014, **4**.

30 C. Chang, V. H. Tran, J. Wang, Y.-K. Fuh and L. Lin, *Nano lett.*, 2010, **10**, 726-731.

31 B. J. Hansen, Y. Liu, R. Yang and Z. L. Wang, *ACS nano*, 2010, **4**, 3647-3652.

32 D. Mandal, S. Yoon and K. J. Kim, *Macromol. Rapid Commun.*, 2011, **32**, 831-837.

33 J. Fang, H. Niu, H. Wang, X. Wang and T. Lin, *Energy Environ. Sci.*, 2013, **6**, 2196-2202.

34 Y.-K. Fuh, J.-C. Ye, P.-C. Chen and Z.-M. Huang, *J. Mater. Chem. A*, 2014, **2**, 16101-16106.

35 V. Cauda, G. Canavese and S. Stassi, *J. Appl. Polym. Sci.*, 2015, **132**.

36 S. Oh, Y. Kim, Y. Y. Choi, D. Kim, H. Choi and K. No, *Adv. Mater.*, 2012, **24**, 5708-5712.

37 V. Cauda, S. Stassi, K. Bejtka and G. Canavese, *ACS Appl. Mater .Interfaces*, 2013, **5**, 6430-6437.

38 C.-C. Hong, S.-Y. Huang, J. Shieh and S.-H. Chen, *Macromolecules*, 2012, **45**, 1580-1586.

39 V. Cauda, B. Torre, A. Falqui, G. Canavese, S. Stassi, T. Bein and M. Pizzi, *Chem. Mater.*, 2012, **24**, 4215-4221.

40 D. Guo, X. Chen, X. Chu, F. Zeng, Y. Bai, J. Cao and B. Dkhil, *J. Appl. Phys.*, 2013, **113**, 187210.

41 H. Tian, J. Shao, Y. Ding, X. Li and H. Liu, *Langmuir*, 2013, **29**, 4703-4714.

42 K. Lau, Y. Liu, H. Chen and R. Withers, *Adv. Condens. Matter Phys.*, 2013, **2013**.

43 L. Persano, C. Dagdeviren, Y. Su, Y. Zhang, S. Girardo, D. Pisignano, Y. Huang and J. A. Rogers, *Nat. Commun.*, 2013, **4**, 1633.

44 K. J. Kim, N. M. Reynolds and S. L. Hsu, *Macromolecules*, 1989, **22**, 4395-4401.

45 V. Sencadas, R. Gregorio Jr and S. Lanceros-Méndez, *J. Macromol. Sci.*, 2009, **48**, 514-525.

46 V. Bhavanasi, D. Y. Kusuma and P. S. Lee, *Adv. Energy Mater.*, 2014, 4.

47 P. Cebe and J. Runt, *Polymer*, 2004, **45**, 1923-1932.

48 Y.-S. Lee, G. Collins and T. L. Arinzeh, *Acta. Biomater.*, 2011, **7**, 3877-3886.

49 G. Canavese, S. Stassi, V. Cauda, A. Verna, P. Motto, A. Chiodoni, S. L. Marasso and D. Demarchi, *Sensors Journal, IEEE*, 2013, **13**, 2237-2244.

50 X. Chen, Y. Wang, K. Cai, Y. Bai, S. Bo and D. Guo, *J. Appl. Phys.*, 2014, **116**, 066821.

51 D. Guo, I. Stolichnov and N. Setter, *J. Phys. Chem. B*, 2011, **115**, 13455-13466.

52 Y. Ma, W. Hu, J. Hobbs and G. Reiter, *Soft Matter*, 2008, **4**, 540-543.

53 M. Steinhart, P. Göring, H. Dernaika, M. Prabhukaran, U. Gösele, E. Hempel and T. Thurn-Albrecht, *Phys. Rev. Lett.*, 2006, **97**, 027801.

54 J. L. Lutkenhaus, K. McEnnis, A. Serghei and T. P. Russell, *Macromolecules*, 2010, **43**, 3844-3850.

55 W. H. Liew, M. S. Mirshekarloo, S. Chen, K. Yao and F. E. Tay, *Sci. Rep.*, 2015, **5**, 9790.

56 Z. Hu, M. Tian, B. Nysten and A. M. Jonas, *Nat. mater.*, 2009, **8**, 62-67.

57 D. Guo, F. Zeng and B. Dkhil, *J. Nanosci. Nanotechno.*, 2014, **14**, 2086-2100.

58 D. Guo and N. Setter, *Macromolecules*, 2013, **46**, 1883-1889.

59 D. Guo, S. Ikeda, K. Saiki, H. Miyazoe and K. Terashima, *J. Appl. Phys.*, 2006, **99**, 094502.

60 R. A. Whiter, V. Narayan and S. Kar-Narayan, *Adv. Energy Mater.*, 2014, **4**, 1400519.

61 F.-R. Fan, L. Lin, G. Zhu, W. Wu, R. Zhang and Z. L. Wang, *Nano lett.*, 2012, **12**, 3109-3114.

62 Z. L. Wang, *ACS nano*, 2013, **7**, 9533-9557.

63 X. Chen, H. Tian, X. Li, J. Shao, Y. Ding, N. An and Y. Zhou, *Nanoscale*, 2015, **7**, 11536-11544.

64 S. Cha, S. M. Kim, H. Kim, J. Ku, J. I. Sohn, Y. J. Park, B. G. Song, M. H. Jung, E. K. Lee and B. L. Choi, *Nano lett.*, 2011, **11**, 5142-5147.

65 S. M. Kim, J. I. Sohn, H. J. Kim, J. Ku, Y. J. Park, S. N. Cha and J. M. Kim, *Appl. Phys. Lett.*, 2012, **101**, 013104.

66 N. Cui, L. Gu, J. Liu, S. Bai, J. Qiu, J. Fu, X. Kou, H. Liu, Y. Qin and Z. L. Wang, *Nano Energy*, 2015, **15**, 321-328.

Table of contents entry

Self-powered Flexible Pressure Sensors with Vertically Well-aligned Piezoelectric Nanowire Arrays for Vital Signs Monitoring

Xiaoliang Chen,[a] Jinyou Shao,*[a] Ningli An,*[b] Xiangming Li,[a] Hongmiao Tian,[a] Chuan Xu[a] and Yucheng Ding[a]

[a]Micro- and Nano-technology Research Center, State Key Laboratory for Manufacturing Systems Engineering, Xi'an Jiaotong University, Xi'an, Shaanxi 710049, China

[b]College of Printing and Packaging Engineering, Xi'an University of Technology, Xi'an, Shaanxi 710048, China

*Corresponding author: jyshao@mail.xjtu.edu.cn(Jinyou Shao)& annl@xaut.edu.cn (Ningli An)

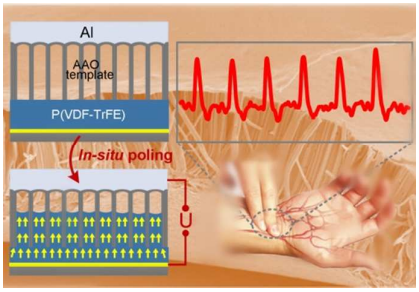

We propose an *in-situ* poling of vertically well-aligned piezoelectric nanowire array with preferential polarization orientation as highly sensitive self-powered sensor for vital signs monitoring.